A Mistuning-Tolerant and Controllable Power Supply for Roadway Wireless Power Systems

Abhilash Kamineni, *Student Member, IEEE*, Michael J. Neath, *Student Member, IEEE*, Grant A. Covic, *Senior Member, IEEE*, and John T. Boys

***Abstract*—Inductive power transfer power supplies for electric vehicle charging in dynamic applications need to tolerate large variations in coupling and tuning with varying loads. This paper investigates the use of a buck converter to regulate the input voltage to a fixed frequency unidirectional switch push–pull converter to meet the requirements of dynamic charging. The presented circuit is optimized to remove some of the additional components introduced. A mathematical model is presented that shows the circuit is capable of operating while extremely mistuned in both the inductive and capacitive regions while maintaining sinusoidal currents. A controller design is also presented allowing constant primary current operation, safe start up, and operation under no load conditions. A 5-kW prototype was built and validated when operated with a dynamic load under severely mistuned conditions.**

***Index Terms*—Highway charging, inductive power transfer, push–pull converter, wireless power transfer.**

I. Introduction

INDUCTIVE power transfer utilizes two loosely coupled inductors (pads) to transfer power over an air gap [1]. In recent years, it has been proposed as a desirable means of charging electric vehicles (EVs) in stationary applications such as in garages and car parks [2]–[4]. There has been a lot of work to standardize these systems with the SAE J2954 committee agreeing to use an operating frequency of 85 kHz [5]. Dynamic charging applications have also been proposed, allowing charging while driving on roads, highways [6]–[8], and train tracks [9]. Several dynamic charging topologies have been proposed including using long tracks embedded in the road [7], [10], [11] or using individual pads that are energized as a vehicle drives over them [8], [9]. Double-coupled systems [6] have also been proposed to avoid having dc or mains buried under the road. Double coupling utilizes a long track operated at a lower frequency to distribute power to several power supplies that selectively energize the charging pads at higher frequencies, based on the proximity of a vehicle on the road.

Dynamic charging applications for highways require power supplies that tolerate operating under a wide range of coupling conditions as an EV moves over the in-ground pad it is driving over. The power supply also has to tolerate varying power demands since small cars require less power and may be lower to the ground compared with large trucks and buses, which usually require more power and have a higher ground clearance. Furthermore, different EV manufacturers may use different tuning topologies in their vehicles, so the primary power supply needs to be able to deal with the varying reflected impedances from these vehicles. The power supply also has to be able to deal with manufacturing tolerances of components and degradation over time, causing the circuits to get further mistuned. A phase synchronized fixed frequency power supply is desirable to prevent interference between neighboring power supplies.

To address these issues, it is necessary to create a power supply that is tolerant to severe mistuning while allowing the current within the primary pad to be controlled to a desirable value. In a previous investigation [12], a push–pull converter with a bank of switchable capacitors was proposed as a solution to these problems by retuning the power supply continuously during operation. While this method was demonstrated to work well, even at high speeds, it required a lot of extra switches and components and lacked the controllability typically found in H-bridge-based topologies.

Topologies utilizing an H-bridge inverter are capable of varying the primary current [13], [14], however, they are usually designed to operate at a fixed duty cycle—either to limit harmonics [15] or to maximize the output power. Additionally, H-bridge-based power supplies often require boost converters to step up the input dc bus voltage to 600–800 V. Push–pull-based topologies are able to operate with a high resonant tank voltage that can be achieved even with a low input dc voltage—meaning it is possible to design a high-power converter with a 300-V dc bus. Furthermore, the push–pull converter switches are referenced to ground, making the circuit easy to drive. However, traditionally with push–pull converters there has been no way to control the primary pad current—it is either ON or OFF, which is one of the reasons this paper focuses on utilizing the buck converter to this desired control.

In this paper, a power supply topology utilizing a buck converter to enable regulation of a unidirectional switch push–pull (USPP) converter [16] has been proposed to keep the circuit working even when mistuned. In practice, any step down dc–dc converter can be used, however, using a buck converter gives the additional benefit of minimizing components when combined with a push–pull converter.

Manuscript received June 30, 2016; revised September 15, 2016; accepted October 19, 2016. Date of publication October 27, 2016; date of current version April 24, 2017. Recommended for publication by Associate Editor C. T. Rim.

The authors are with the Power Electronics Research Group, University of Auckland, Auckland 1142, New Zealand (e-mail: abhilash.kamineni@auckland.ac.nz; m.neath@auckland.ac.nz; ga.covic@auckland.ac.nz; j.boys@auckland.ac.nz).

Color versions of one or more of the figures in this paper are available online at http://ieeexplore.ieee.org.

Digital Object Identifier 10.1109/TPEL.2016.2622300

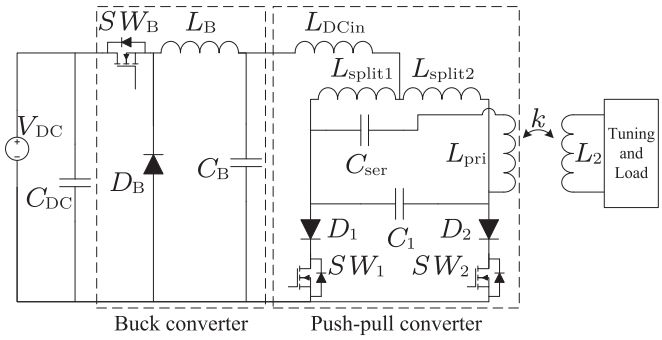

Fig. 1. Generalized proposed topology.

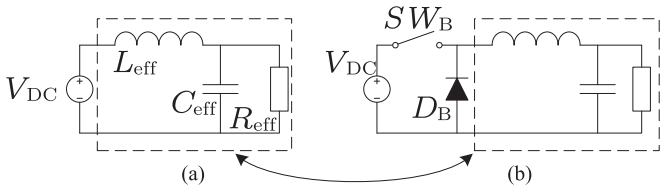

Fig. 2. (a) Transient model of the push–pull converter and (b) buck converter with the filter highlighted.

The paper is structured as follows. In Section II, the proposed topology is presented and is mathematically analyzed in Section III. In Section IV, a suitable control scheme is discussed and is demonstrated in dynamic simulations, followed by experimental results and discussions in Section V. Finally, the conclusions are presented in Section VI.

II. Proposed Topology

The general form of the proposed topology is shown in Fig. 1. In a few feature, it incorporates a buck converter at the input to regulate the voltage into the USPP converter [16]. The buck converter is configured as a standard buck converter, but instead of a load resistor it drives the USPP converter that operates at a fixed frequency rather than under load resonant conditions as has been done in the past [17]. This significantly alters the operation and control of the system. The USPP converter turns the dc input voltage into a quasi-current source using L_{DCin} and the two splitting inductors L_{split1} and L_{split2}. The switching action of the switches SW_1 and SW_2 and their series diodes D_1 and D_2 create an ac current in the primary coil L_{pri}. The capacitors C_{ser} and C_1 tune the primary coil L_{pri}. The secondary coil L_2 is coupled to L_{pri} by the coupling factor k. L_2 is then connected to a tuning capacitor network and a load.

A. Component Minimization

In [18], it was shown that transiently a push–pull converter can be modeled as shown in Fig. 2(a). It can be seen that this matches the filter of the buck converter highlighted in Fig. 2(b). By removing the additional filter, the combined buck and USPP converter can be reconfigured as shown in Fig. 3(a). L_{DCin} shown in Fig. 1 can be removed providing that the independent dc inductors (L_{DC1} and L_{DC2}) are sufficiently large and designed to match the performance of L_{DCin}, L_{split1}, and L_{split2}.

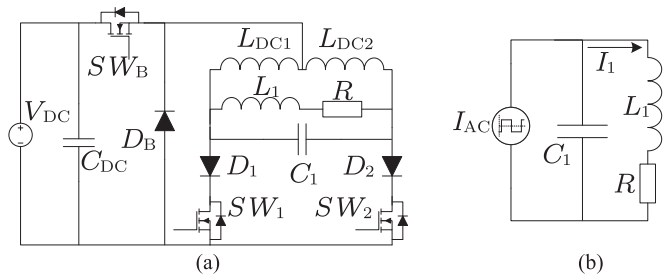

Fig. 3. (a) Modified proposed topology and (b) current injection into push–pull tank.

For the purpose of the following analysis, C_{ser}, L_{pri}, and the reflected impedance of the secondary circuit were simplified and represented by the inductor L_1 in series with a load R. This is to help with understanding how the circuit operates in Section II-B and C, and is mathematically justified in Section III.

B. Operation of the Buck Converter Stage

The buck converter optimization shown in Section II-A is feasible because the dc inductors of the push–pull circuit convert the dc voltage source to a quasi-dc current source that flows through these inductors. Similarly, a buck converter operating in the continuous region has a dc current with a triangle-wave-shaped ripple flowing through its inductor, with the skew of the triangle wave reflecting the duty cycle of the switch. With a sufficiently large filter inductance, the amplitude of this ripple can be minimized.

By replacing the filter of the buck converter with a push–pull converter, the operation will be largely the same. When switch $\mathrm{SW_B}$ is closed, the diode D_{B} does not conduct, and the circuit operates as a normal push–pull converter. When $\mathrm{SW_B}$ is opened, D_{B} starts to conduct and the energy in the dc inductors L_{DC1} and L_{DC2} are drained into the push–pull converter.

C. Operation of the USSP

The USPP converter is operated by driving switches SW_1 and SW_2 180° out of phase with each other with a 50% duty cycle at 85 kHz. The dc inductors L_{DC1} and L_{DC2} turn the voltage input into a quasi-current source, causing a square wave current source I_{AC} to be fed into the *LC* tank as shown in Fig. 3(b). I_{AC} can be directly adjusted by varying the duty cycle of the buck converter switch $\mathrm{SW_B}$.

The diodes in series with the switches (D_1 and D_2) prevent the body diodes of the switches from conducting. In fixed frequency bidirectional switch, push–pull converters such as the one used in [12], D_1 and D_2 are not present so the conduction of the body diodes forces the tank voltage to 0 V each half cycle. This is problematic when the power supply is capacitively tuned because in every half cycle the charged tuning capacitor will be short circuited by the body diode conduction, potentially damaging the switches. Therefore, [12] needs to be designed such that it is inductively tuned over the entire range of operation.

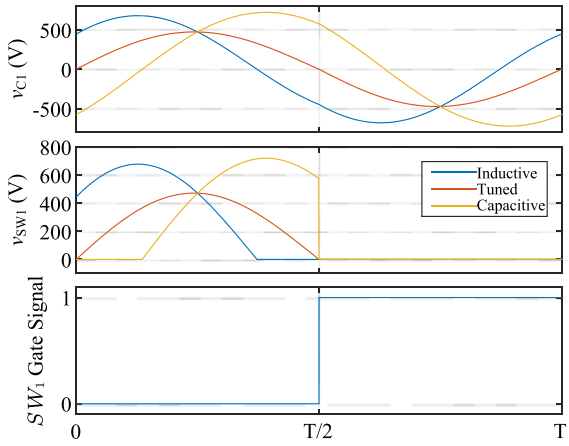

Fig. 4. Tank voltage v_{C1} and switch voltage v_{SW1} variation of a USPP due to $\pm 10\%$ variation in L_1 around the perfectly tuned point.

In the USPP, the tank voltage when mistuned is no longer forced to 0 V when SW_1 and SW_2 switch, resulting in negative voltage swings across each push–pull switch and its series diode every half cycle. The negative voltage swing causes a larger positive voltage swing across the switch, increasing the overall rms tank voltage. This occurs because the mean voltage across each USPP switch and its series diode has to equal the input dc voltage, given the mean voltage across the dc inductors is 0 V at a steady state. The increased tank voltage when mistuned can be seen in Fig. 4. When the circuit is perfectly tuned, the switches are zero voltage switched, resulting in the lowest rms tank voltage.

As the circuit gets mistuned in either direction, the tank voltages increase and the tank voltage waveforms are no longer in phase with the switching, resulting in non-zero volt switching operation and higher currents through the USPP switches and diodes. However, under both inductive and capacitive mistuning conditions, the V_{C1} waveform is still approximately sinusoidal in form and there are no large current or voltage spikes [16], making the circuit usable if the input voltage can be regulated appropriately. In Fig. 4, it can also be seen that the voltage across the switch never goes negative but is clamped by the reverse diode, resulting in at least one edge being zero voltage switched every cycle under all mistuning conditions.

III. Mathematical Model

A. USPP Model

To the mathematical model of the USPP circuit under fixed frequency operation, it is necessary to make some assumptions. First, it is assumed that the extra distortion introduced into the push–pull waveforms by the switching of the buck converter is negligible. The buck converter is modeled by varying the dc input voltage source. Both dc inductors are assumed to be of equal value and all the components are assumed to be lossless. Finally, the secondary circuit can be simplified to a reflected impedance $Z_{\rm ref}$ in series with the primary inductance as shown in [19]. The reflected impedance for parallel- and series-tuned secondaries are given by $Z_{\rm ref-p}$ and $Z_{\rm ref-s}$

$$Z_{\rm ref-p} = \frac{M^2 R_{\rm OUT}}{L_2^2} - j\frac{\omega M^2}{L_2}$$
$$Z_{\rm ref-s} = \frac{\omega^2 M^2}{R_{\rm OUT}} \tag{1}$$

where $R_{\rm OUT}$ is the load resistance and M is the mutual inductance between the primary and secondary coils given by $k\sqrt{L_{\rm pri}L_2}$. Using $Z_{\rm ref}$ values from (1), the equivalent inductance L_1 and resistance R driven by the power supply as shown in Fig. 3(a) can be calculated by summing the impedances of $L_{\rm pri}$, $C_{\rm ser}$, and $Z_{\rm ref}$. The equivalent inductance and resistance with a parallel-tuned secondary are given by

$$L_1 = L_{\rm pri} - \frac{1}{\omega^2 C_{\rm ser}} + \frac{\Im(Z_{\rm ref-p})}{\omega} = L_{\rm pri}(1-k^2) - \frac{1}{\omega^2 C_{\rm ser}} \tag{2}$$

$$R = \Re(Z_{\rm ref-p}) = \omega L_{\rm pri} k^2 Q_{\rm LOAD}. \tag{3}$$

Similarly, the equivalent inductance and resistance when using a series-tuned secondary are given by

$$L_1 = L_{\rm pri} - \frac{1}{\omega^2 C_{\rm ser}} \tag{4}$$

$$R = \Re(Z_{\rm ref-s}) = \omega L_{\rm pri} k^2 Q_{\rm LOAD}. \tag{5}$$

In (2)–(5), L_1 and R are the equivalent primary inductance and resistance of the push–pull converter as shown in Fig. 3(a). $L_{\rm pri}$ is the actual primary coil inductance, ω is the frequency of switching, $C_{\rm ser}$ is the value of any series capacitance used for tuning, k is the coupling between primary and secondary coils, and $Q_{\rm LOAD}$ is the loaded quality factor of the secondary that can be adjusted to regulate the output power. $Q_{\rm LOAD}$ is given by $R_{\rm OUT}/\omega L_2$ for a parallel-tuned secondary and $\omega L_2/R_{\rm OUT}$ for a series-tuned secondary.

It should also be noted that in (2)–(5) and for the rest of Section III, no specific details about the magnetic design such as the pad topology, air gap, or size of the magnetic pads is considered. This is because these physical properties are represented as pad inductances ($L_{\rm pri}$ and L_2) and coupling factor k in an electrical system. The physical characteristics such as pad topologies and the shape of the coupling profile curve will, however, be considered in Sections IV and V for the dynamic system under evaluation, linked specifically to the topologies used in that case.

Using these assumptions, the simplified circuit that is modeled is shown in Fig. 3(a) except that a variable dc voltage source is connected directly to the USPP. The assumptions allow the circuit to be represented as two third-order systems that switch between each other as shown in Fig. 5(a) and (b). The third-order circuit in Fig. 5 can be represented by the following

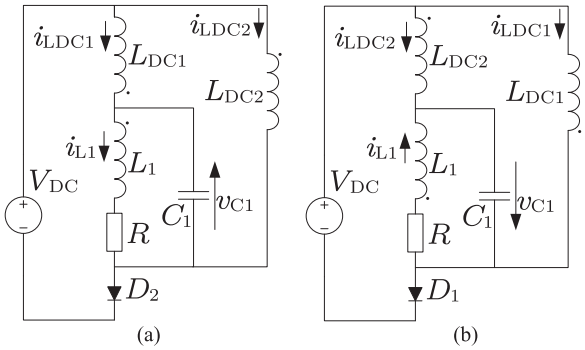

Fig. 5. Equivalent circuit for (a) t = 0 to t = T/2 and (b) t = T/2 to t = T.

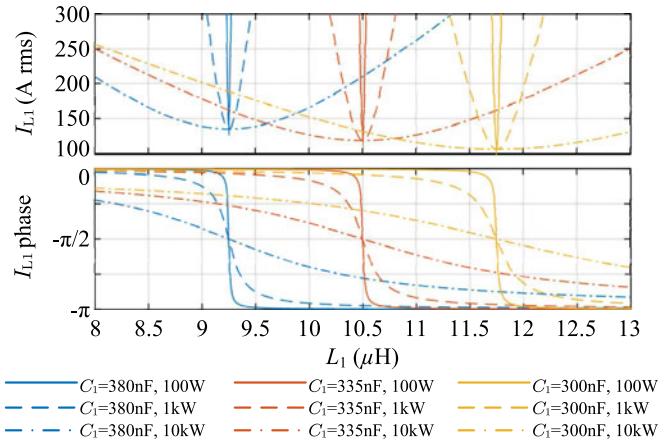

Fig. 6. Primary current amplitude and phase variation as tuning capacitance, primary inductance, and load vary with no buck converter regulation.

differential equation:

$$\frac{RV_{\mathrm{DC}}}{L_{\mathrm{DC}}L_1C_1} = \frac{\mathrm{d}^3v_{\mathrm{C1}}}{\mathrm{d}t^3} + \frac{R}{L_1}\frac{\mathrm{d}^2v_{\mathrm{C1}}}{\mathrm{d}t^2} + \left(\frac{1}{L_1C_1} + \frac{1}{L_{\mathrm{DC}}C_1}\right)\frac{\mathrm{d}v_{\mathrm{C1}}}{\mathrm{d}t} + \frac{R}{L_{\mathrm{DC}}L_1C_1}v_{\mathrm{C1}}. \tag{6}$$

The time domain representation of i_{LDC}, i_{L1}, and v_{C1} can be obtained by solving (6). The solutions are valid for $t = 0$ to $t = T/2$ and can be written in the form of

$$w(t) = a_1e^{-\beta t} + e^{-\alpha t}\left(a_2\cos(\omega_{\mathrm{d}}t) + a_3\sin(\omega_{\mathrm{d}}t)\right) + a_4 \tag{7}$$

where $w(t)$ is the general form of the waveform of i_{LDC}, i_{L1}, and v_{C1}. β is the real root of the characteristic equation of (6), and α and ω_{d} are the real and imaginary parts, respectively, of the complex root of the characteristic equation. The values of the constants a_1, a_2, a_3, and a_4 can be found using the input dc voltage, initial current of the inductors, and the initial voltage of the tuning capacitor. Since the diodes D_1 and D_2 block the body diodes of SW_1 and SW_2 from conducting, the boundary conditions are given as

$$\begin{aligned} v_{\mathrm{C1}}(t=0) &= -v_{\mathrm{C1}}\left(t=\frac{T}{2}\right) \\ i_{\mathrm{L1}}(t=0) &= -i_{\mathrm{L1}}\left(t=\frac{T}{2}\right) \\ i_{\mathrm{LDC}}(t=0) &= i_{\mathrm{LDC}}\left(t=\frac{T}{2}\right) + \frac{V_{\mathrm{DC}}\frac{T}{2}}{L_{\mathrm{DC}}}. \end{aligned} \tag{8}$$

B. Push–Pull Performance With No Regulation

Using the model presented in Section III-A, the performance of the circuit without a dc/dc converter to adjust the input voltage can be examined to see why the proposed buck converter is necessary.

Fig. 6 shows how the behavior of the circuit changes due to variations in L_1 as the tuning capacitance and load change. These variations are representative of variations in coupling and loading from a secondary side as shown in (2)–(5). On these graphs, the minima in I_{L1} indicate when the circuit is perfectly tuned. The equivalent load resistance R is chosen to achieve the specified output power at the tuned points and is used for the rest of that sweep for each curve. To put the large currents shown in Fig. 6 into prespective, in the simulated circuit most of the component ratings have been exceeded by the time I_{L1} exceeds 150 A, even when using 1200-V rated devices.

It can be seen that under lightly loaded conditions, the circuit becomes more sensitive to mistuning as indicated by the rapidly rising currents and the sharper phase plots. Although it has been shown that retuning a converter during operation in a dynamic system is possible [12], most EV charging applications still use designs that are perfectly tuned at just one desired operation point in order to minimize the number of components used. Thus, if fixed tuning scenario is used, it is safe to assume that the circuit will almost always be operating under mistuned conditions, especially at light load, so a buck converter is required to regulate the input voltage in order to maintain an appropriate I_{L1} and protect the components from exceeding their ratings.

However, despite the voltages and currents in the system becoming extremely large, the total harmonic distortion in the track current has remained low [16]—peaking at a maximum of 2.5% when mistuned and approximately 0.25% under ideal tuning conditions.

C. Buck Converter Regulation Impact on Efficiency

In Section III-A, a mathematical model was developed that allows the USPP to be evaluated. Using this model, it was shown in Section III-B that a buck converter is required to regulate the input voltage of the USPP to keep it operating in a safe region. However, before the regulated performance of the USPP is considered, it is necessary to look at the operation of the buck converter and its impact on the converter losses.

The dc and switching current pathways from the input current through the switch currents are shown in Fig. 7 when SW_1 is closed and SW_2 is open. In the other half cycle, when SW_2 is closed and SW_1 is open, I_{SWPP} flows through SW_2 and no current flows through SW_1. I_{IN} is a dc current whose magnitude is given as

$$I_{\mathrm{IN}} = \frac{P_{\mathrm{IN}}}{V_{\mathrm{DC}}} \tag{9}$$

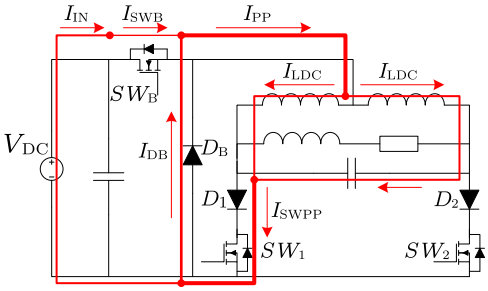

Fig. 7. Pathway of currents of interest through the circuit when SW_1 is closed and SW_2 is open.

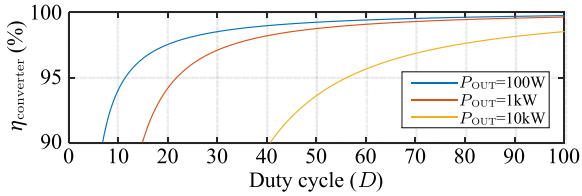

Fig. 8. Variation in $\eta_{converter}$ due to changes in the duty cycle of SW_B.

where P_{IN} is the total input power to the system. Using standard buck converter and push–pull converter equations, the following relationships can be written:

$$I_{PP} = \frac{I_{IN}}{D} = \frac{I_{SWB}}{\sqrt{D}} = \frac{I_{DB}}{\sqrt{(1-D)}} = 2I_{LDC} = \sqrt{2}I_{SWPP} \tag{10}$$

where I_{IN}, I_{PP}, and I_{LDC} are dc currents and I_{SWB}, I_{DB}, and I_{SWPP} are rms currents as indicated on Fig. 7. D is the duty cycle of SW_B while SW_1 and SW_2 are driven 180° out of phase at a fixed duty cycle of 50%. It is assumed that C_{DC} and the dc inductors L_{DC1} and L_{DC2} are large enough so that the ripple voltages and currents are negligible for this analysis.

From (10), it can be seen that the currents through the dc inductors and semiconductor devices depend on the duty cycle D of the buck converter. As the circuit gets mistuned, the primary current I_1 increases as shown in Fig. 6. The controller compensates for this mistuning by decreasing the duty cycle of SW_B, however, the output power has not changed during this process. Thus, the losses in just the proposed push–pull converter can be analyzed. For this analysis, the switching losses are not considered since approximately 80%–90% of the losses in the inverter circuit are conduction losses. The conduction losses in the individual components are

$$\begin{aligned} P_{SWB} &= I_{PP}^2 R_{onSW} D \\ P_{DB} &= \left(I_{PP} V_f + I_{PP}^2 R_{onD}\right)(1-D) \\ P_{SW1} &= P_{SW2} = I_{SWPP}^2 R_{onSW} \\ P_{D1} &= P_{D2} = \frac{I_{SWPP} V_f}{\sqrt{2}} + I_{SWPP}^2 R_{onD} \\ P_{LDC1} &= P_{LDC2} = I_{LDC}^2 R_{LDC} \end{aligned} \tag{11}$$

where R_{onSW} and R_{onD} are the ON state resistances of the switches and diodes, respectively, V_f is the forward voltage drop of the diodes at low currents, and R_{LDC} is the ESR of the dc inductors L_{DC1} and L_{DC2}.

The total conduction loss in the converter expressed in terms of I_{IN} is given as

$$P_{Loss} = \frac{I_{IN} V_f}{D}(2-D) + \frac{I_{IN}^2}{D^2}\left(R_{onSW}(1+D) + R_{onD}(2-D) + \frac{R_{onLDC}}{2}\right) \tag{12}$$

which can be rewritten in the form of a quadratic equation

$$P_{Loss} = AI_{IN}^2 + BI_{IN} \tag{13}$$

where $A = D^{-2}(R_{onSW}(1+D) + R_{onD}(2-D) + 0.5R_{onLDC})$ and $B = V_f D^{-1}(2-D)$.

Thus, the total input power can be written as

$$P_{IN} = P_{OUT} + P_{Loss} \tag{14}$$

where P_{OUT} is the total output power including the losses in the primary resonant tank as well as all the secondary components. By equating (9) and (14), the following quadratic equation is obtained:

$$0 = AI_{IN}^2 + (B - V_{DC})I_{IN} + P_{OUT}. \tag{15}$$

which can be solved to obtain I_{IN} and hence P_{IN} and P_{Loss}. Therefore, the efficiency of the proposed converter when considering just the conduction losses for a given input voltage V_{DC} and output power P_{OUT} is given as

$$\eta_{converter} = \frac{P_{OUT}}{P_{IN}}. \tag{16}$$

The variation in $\eta_{converter}$ is shown in Fig. 8 at various values of P_{OUT}. To generate this figure, V_{DC} was set to 300 V, R_{onSW} = 25 mΩ, R_{onD} = 45 mΩ, and V_f = 0.7 V. These component specifications are typical of what can be expected with good quality 1200-V SiC switches and diodes available today. It can be seen that at a low-duty cycles and high power levels the efficiency of the converter starts to quickly drop off. Thus, to maintain the losses in the converter to a manageable amount, a minimum $\eta_{converter}$ of 95% should be targeted that restricts the duty cycle of SW_B to a minimum of 56% for an output power of 10 kW. This restriction on the duty cycle places a restriction on how much mistuning the converter can handle, so the tuning should be selected appropriately.

D. Push–Pull Performance With Buck Converter Input Regulation

When selecting the components values for the circuit there are several factors that need to be considered. The three main factors—inductance variations, C_{ser} selection, and C_1 selection is discussed followed by an examination of how the circuit behaves with the buck converter regulation.

1) Inductance Variations: In this simulation, a primary pad L_{pri} with an inductance that varies between 81.7 μH with no secondary pad ($k = 0$) and 85.8 μH ($k = 0.23$) when the secondary pad is centered on top of the primary pad. These specifications are similar to those used for the experimental system—which is why they are chosen here. The inductance increases because of

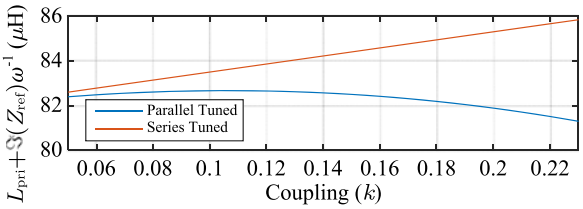

Fig. 9. Variation in inductance measured across the primary coil due to reflected impedances from series- and parallel-tuned secondaries as well as fluctuations in $L_{\rm pri}$.

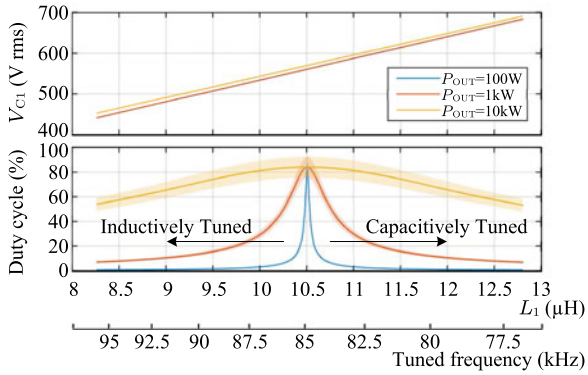

Fig. 10. Variation in $V_{\rm C1}$ and duty cycle of $\rm SW_B$ as coupling and load varies with $I_{\rm L1}$ regulated to 100 A. The duty cycle envelope represents the duty cycle change required for a ±10% variation in $I_{\rm L1}$.

the closer proximity of the ferrite in the primary and secondary pads [20]. This change in $L_{\rm pri}$ as the coupling k varies can be approximated as $(81.7 + 18k)$ μH. The total inductance that needs to be tuned by $C_{\rm ser}$ and C_1 after accounting for variations in $L_{\rm pri}$ and variations in reflected impedances from the secondary are given by the $L_{\rm pri}(1-k^2)$ term in (2) when a parallel tuned secondary is used and $L_{\rm pri}$ as shown in (4) when a series tuned secondary is used. Thus, the full range of inductance that the power supply needs to be able to tune and operate over is 81.3–85.8 μH as shown in Fig. 9.

2) $C_{\rm ser}$ Selection: The tuning capacitor $C_{\rm ser}$ is selected to ensure that the primary current $I_{\rm L1}$ is sufficiently high while restraining the maximum tank voltage $V_{\rm C1}$ and the voltage across the switches and diodes. For this power supply, a primary current of 100 A is required and it is desirable to restrict $V_{\rm C1}$ to 700 Vrms to ensure that the peak voltage across the switches and diodes does not exceed 1 kV. A 48-nF capacitance for $C_{\rm ser}$ is sufficient to restrain the worst-case inductance of 85.8 μH within these limits. Therefore, using (2) and (4), the value of C_1 should be selected to tune an inductance range of 8.26–12.8 μH.

3) C_1 Selection: C_1 should be selected to ensure the duty cycle of the buck converter switch is within the desired range described in Section III-C. This is best achieved by tuning C_1 to the center point of the expected range of variation in L_1 so that only the extremes are potentially operating at undesirably low duty cycles. In this case, a 335-nF capacitance was selected to tune to the midpoint inductance of 10.5 μH.

Using the values of tuning capacitors selected above, Fig. 10 shows a simulation of how the amplitude of the tank voltage $V_{\rm C1}$ varies when a buck converter is used to regulate the primary track current to 100 A with an input voltage $V_{\rm DC}$ of 300 V. The output power was adjusted by varying the equivalent real reflected resistance R [shown in (3) and (5)] from 0.01 to 0.1 Ω and then 1 Ω representing a 100 W, 1 kW, and 10 kW load, respectively. This simulation also highlights why it is necessary for the power supply to tolerate operation in both the inductive and capacitive regions. If C_1 was selected so that it was tuned to one of the extremes—either 8.26 or 12.8 μH — instead of the midpoint of this range then the power supply will be operating extremely inefficiently when mistuned.

Comparing Fig. 6 with 10, it can be seen that regulating the track current limits the amplitude of the tank voltage significantly, allowing safe operation over a wide range of inductances. The envelopes that show the variation in duty cycle required to achieve a ±10% variation in $I_{\rm L1}$ indicate that primary current is extremely sensitive to variations in the duty cycle of the buck converter when operating at low power levels. It can also be seen that the duty cycle peaks at the tuned inductance of 10.5 μH at all three power levels. This is because at this point, the circuit is tuned perfectly so the circuit can operate at its maximum duty cycle. As the circuit is mistuned, $I_{\rm L1}$ will increase as shown in Fig. 6, so the buck converter will need to reduce the duty cycle in order to keep $I_{\rm L1}$ constant. It should be noted that the duty cycle of the buck converter is used to adjust the input current $I_{\rm AC}$ fed into the *LC* tank as shown in Fig. 3(b), not the tank voltage directly.

The peak duty cycle also does not exceed 85% in Fig. 10 to maintain the 100 A regulation. Here with the push–pull converter, the rms tank voltage $V_{\rm C1}$ under tuned conditions can be approximated by $\pi V_{\rm DC}/\sqrt{2} \approx 670$ V in this application. Since $C_{\rm ser}$ was selected to ensure that $V_{\rm C1}$ does not exceed 700 V with $I_{\rm L1} = 100$ A at the worst-case inductance of $L_1 = 12.8$ μH, $V_{\rm C1}$ is limited to just 570 V at the tuned point of $L_1 = 10.5$ μH. If C_1 was tuned to $L_1 = 12.8$ μH then 100% duty cycle would be observed at that point, however, at $L_1 = 8.26$ μH the duty cycle will be below 40% which is undesirable.

E. Limits of Mistuning

From Figs. 8 and 10, the tolerance to mistuning is achieved by sacrificing converter efficiency. This is similar to the way all H-bridge-based topologies also achieve tolerance to mistuning. In Section III-D, it can be seen that the maximum coupling factor considered was $k = 0.23$. If operation at higher coupling factors or larger variations in inductances is desired, then the duty cycle at 10 kW load on Fig. 10 will drop below the desirable 56% shown in Fig. 8, as discussed in Section III-C. In this case, more efficient components will need to be selected or multiple components will need to be paralleled in order to reduce the losses in the circuit to maintain a reasonable efficiency under all tuning conditions.

The circuit also requires the total effective inductance L_1 to be inductive. Under extreme conditions, it is possible for a capacitive reflected impedance to completely tune out L_1. Under such cases, measuring the impedance across the terminal of $L_{\rm pri}$ with an *LCR* meter would give a capacitive reading. As such there is no inductance in the resonant tank, creating undesirable waveforms in the primary pad that are no longer sinusoidal.

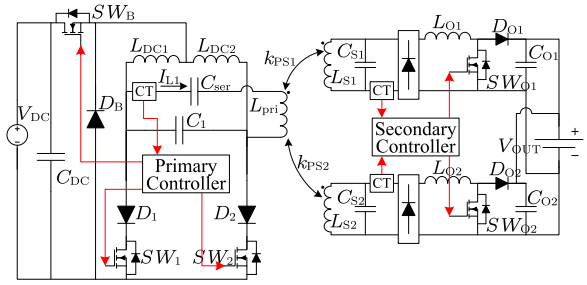

Fig. 11. Full system to be simulated including the control inputs and outputs (red arrows).

TABLE I
COMPONENT VALUES USED IN EXPERIMENTAL SYSTEM

L_{pri}	82.8–85.02 μH	C_1	406.75 μH	C_{ser}	50.39 nF
L_{S1}	10.46–10.53 μH	L_{DC1}	615.38 μH	L_{DC2}	628.20 μH
L_{S2}	10.90–11.06 μH	C_{S1}	334.14 nF	C_{S2}	331.07 nF
$L_{O1,2}$	170 μH	C_{O1}	1200 μF	C_{O2}	2400 μF
V_{DC}	300 V	V_{OUT}	300 V		

IV. CONSTANT CURRENT CONTROL

The prototype system under evaluation and used for experimental evaluation later in Section V is shown in Fig. 11. This system uses a Double D (DD) primary pad [21] (L_{pri}) that is energized by the proposed power supply. A bipolar pad [22], [23], which features two decoupled coils (L_{S1} and L_{S2}) with individual switching rectifiers [24] for each coil, is used to regulate the output current (and hence output power) into a battery. The component values used are listed in Table I. Constant current control of the primary pad current I_{L1} in this prototype has been implemented by monitoring the primary pad current I_{L1} with a current transformer as shown in Fig. 11. Having the primary controller maintain an approximately constant primary current allows the secondary electronics to regulate the output power without fighting the primary controller, and simplifies the secondary controller design.

The primary controller block in Fig. 11 utilizes a proportional integral (PI) controller to adjust the duty cycle of SW_B to ensure that the primary current is regulated to 100 A rms. SW_1 and SW_2 are driven at 85 kHz with a 50% duty cycle. SW_B was also driven at 85 kHz so that any distortion in the waveforms due to the buck converter operation is consistent per cycle. This form of control is enough to ensure that the tank voltage V_{C1} is within safe limits, as seen in Fig. 10. If necessary, an additional peak voltage detection circuit can be added to guarantee that the switch ratings are not exceeded.

In this circuit, switching secondary regulators are used to regulate the output current that flows into the battery from each coil of the bipolar secondary pad. The regulators use the well-known boost converter configuration [24] to monitor the short-circuit current from each coil with current transformers and adjust the duty cycle of SW_{O1} and SW_{O2} as necessary. In the simulation, both switches are driven at the same duty cycle, however, they can also be driven at different duty cycles in order to minimize the losses in L_{S1} and L_{S2}. This gives flexibility for prototyping and experimental evaluations, however, in an optimized system the output of the two diode bridge rectifiers would be connected and only one boost-type regulator would be used for both coils.

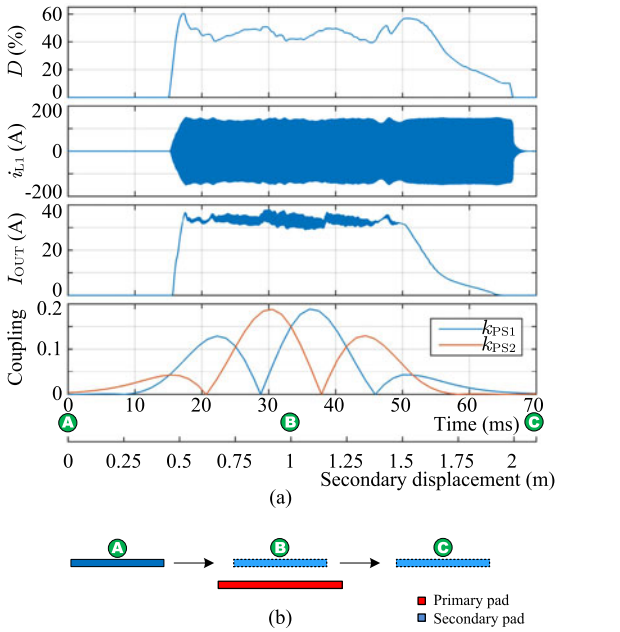

Fig. 12. (a) Dynamic simulation of the system showing regulation I_{L1} as the secondary moves at 100 km/h and (b) position of the moving secondary pad relative to the primary pad at various points in the simulation.

A PLECs simulation of the full system with the secondary pad moving over the primary pad at 30 ms^{-1} (108 km/h) is shown in Fig. 12(a). This speed is the expected maximum speed for a vehicle on an electrified highway indicating that the proposed control scheme is fast enough to regulate the system. The position of the secondary pads relative to the primary pad at the start, middle, and end of the simulation has also been shown in Fig. 12(b) to help visualize the movement of the secondary pad. A 300-V battery is used as the load and the output current I_{OUT} regulated to approximately 33 A in order to ensure a constant 10-kW power transfer. During this time, the primary current was successfully regulated to approximately 100 $\pm$ 20 A rms as expected by adjusting the duty cycle D of SW_B.

Note that the power supply is turned ON at 15 ms in the simulation and the controller ramps the primary current up with almost no overshoot. Such a signal to turn ON the power supply can be obtained by using a detection scheme such as those proposed in [25]–[28]. At a displacement of 1 m, the secondary pad is centered over the vehicle pad and at displacements beyond 1.5 m, the secondary pad is significantly misaligned. Typically, the power supply would be shut OFF after this displacement and the next power supply on the highway would be expected to energize the secondary pad, however, to demonstrate the ability of the power supply to continue to operate safely at low loads it was left ON for an extra 15 ms as the output power drawn decreased.

A. Constant Current Control With a Switching Secondary Regulator

The design of the control algorithm requires extra filtering if the secondary uses switching regulators rather than a passive filter—both of which are used in practice with the choice

based on cost and efficiency requirements. The switching from a secondary regulator such as the those in Fig. 11 can cause the reflected impedance on the primary side to vary. The secondary controller adjusts the duty cycle of the output switches SW_{O1} and SW_{O2} to control the current flowing into the load. When the switches are closed, the secondary coils are effectively short circuited and the load is disconnected from the rest of the circuit. Consequently, the power supply will effectively be driving no load at this point, causing the primary current to start increasing. When the output switches open, the power supply will start to drive the load once again and the primary current will decrease.

The secondary regulator switches can operate at frequencies as low as 10–20 kHz and under such situations this creates a ripple in the primary current lasting several cycles. The ripple needs to be filtered out from the current readings on the primary controller otherwise it may try to unsuccessfully compensate for the ripple resulting in large, unstable oscillations in the primary current as the primary and secondary controllers "fight" each other. With appropriate filtering, there will be a small ripple in the primary current, however, the average value will be kept constant.

The primary controller can also be designed to compensate for the switching action of the secondary and eliminate the ripple from the primary current—especially in stationary systems where the duty cycle of the secondary regulator is relatively constant. This, however, requires a deeper investigation and is not within the scope of this paper, given the target here is to supply power under fast varying dynamic applications.

B. Constant Current Control With a Passive Secondary

If the secondary side is a passive filter, then the reflected impedance only varies due to the changes in coupling or L_{pri}. The controller does not require any additional filtering since these variations will be much slower than the switching of an active regulator.

C. Start Up

Typically push–pull converters are difficult to start because they suffer from significant tank voltage and current overshoots. This is because they have no way to regulate the primary current—the power supply is either ON or OFF. One of the benefits of having the buck converter at the input of the USPP is that the circuit can be easily started under controlled conditions to achieve minimal transient ripple by ramping the duty cycle of the buck converter switch. This is demonstrated in Fig. 13(a) where the power supply is able to start up in under 200 μs under load by using a simple PI controller, which is well within the 2 ms advance notice of an upcoming vehicle given by the detection scheme proposed in [25].

If the primary pad is starting under unknown load conditions (in the worst case it may be either no load or full load), then extra precautions need to be taken with the controller design. When energizing an unloaded system, the system is prone to oscillations and overshoots if the controller gains are not carefully chosen. A duty cycle of just 10.5% is required to achieve a track current of 100 A under no load conditions as shown in Fig. 13. Consequently, the controller should be designed so that it checks the magnitude of the I_{L1} at a low-duty cycle of approximately 5% to see if a load is present. At this fixed duty cycle, the magnitude of I_{L1} detected under loaded conditions will be much smaller than at no load so that a controller with lower gains should be used at no load because of the low damping so that it starts up more gradually. This load checking is demonstrated in Fig. 13—in both scenarios the controller sets the duty cycle to 5% for 200 μs to check if a load is present. In Fig. 13(a), a load is detected and the duty cycle of the buck converter is increased rapidly. However, in Fig. 13(b) no load is detected causing the controller to use lower gains so that the circuit starts up more gradually.

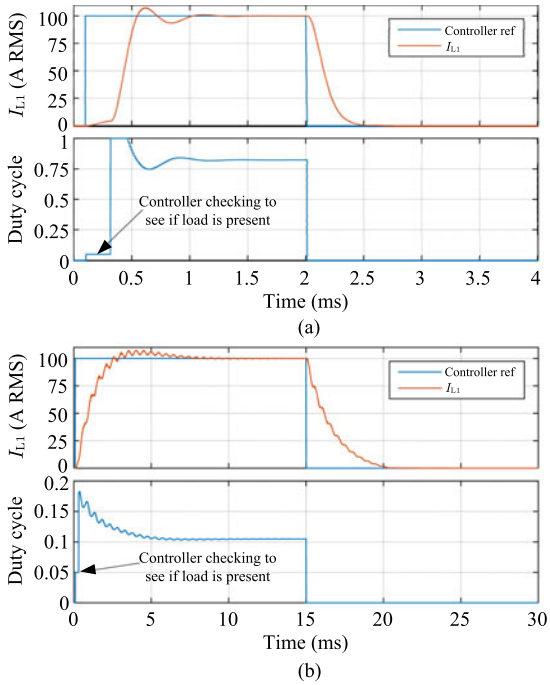

Fig. 13. PLECs simulation of the system showing regulation start up and shut down of the power supply under (a) loaded conditions and (b) no load conditions.

D. Shut Down and Fault Conditions Triggered by the Secondary

To shut down the power supply, the buck converter switch can simply be opened at any time and this will stop injecting energy in the resonant tank as shown in Fig. 13(a) and (b). Here, the buck converter duty cycle was instantly set to zero at 2 and 15 ms, respectively. The energy stored in the dc inductors will be dissipated in the *LC* tank and the buck converter diode D_{B} will provide a return pathway for these inductors. It is important to note that the push–pull converter switches SW_1 and SW_2 still need to continue commutating until all of the energy in the *LC* tank and the dc inductors has been dissipated. If SW_1 and SW_2 were to be opened immediately then the energized dc inductors would be open circuited, which would create a large transient voltage across the terminals of the dc inductors and damage all the components connected to them.

Additionally, it is important for the controller to react to appropriately to the fault conditions created by the secondary electronics. Many secondary regulators often have additional

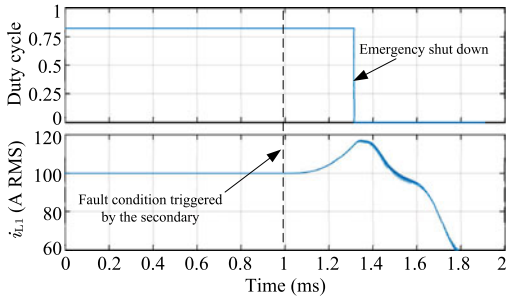

Fig. 14. PLECs simulation of the system showing increasing currents when the load is removed and the emergency shut down needed to protect the circuit.

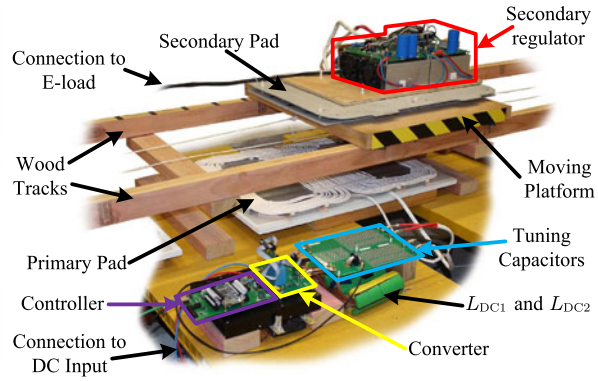

Fig. 15. Experimental setup of the 5-kW dynamic charging prototype.

protection circuitry that allows the load to be completely disconnected from the power supply—usually by opening or short circuiting the secondary coil. For example, this can be implemented by having a crowbar circuit across the output switches SW_{O1} and SW_{O2} in Fig. 11. When a fault condition is detected, the crowbar circuit will instantly close across the switch. This results in a sudden drop of the load on the power supply. The controller in the power supply has to be able to react to this immediately and open the buck switch SW_B so that no more energy is injected into the *LC* tank of the push–pull converter.

To demonstrate this, the peak primary current is plotted in Fig. 14. A fault condition was triggered in the secondary side at 1 ms that causes the secondary regulator to shed its load instantaneously. To demonstrate the exponential increase in I_{L1}, the duty cycle was held constant from 1 to 1.31 ms. At this time, I_{L1} exceeded a predefined overcurrent threshold—in this case 115 A, causing the controller to shut itself OFF to protect the circuit. In a practical system, the controller would start to reduce the duty cycle between 1 and 1.31 ms, however, since the current rises exponentially, often the controller will not be able to reduce it enough—especially since controller gains tend to be lowered near steady state to prevent hunting. If the controller did not perform the hard shut off as shown in Fig. 14 then the primary current would continue to increase rapidly, which has the potential to damage not only the power supply but also the secondary crowbar circuit because it is still coupled to the primary coil. In practice, an overcurrent safety feature can be implemented either in the software or with dedicated hardware using a comparator circuit to detect such a fault condition.

V. Experimental Results and Discussions

To test the operation of the proposed power supply under dynamic operation, a 5-kW prototype shown in Fig. 15 was built and the component values used are listed in Table. I. The primary pad used was a 775 × 600 mm DD pad, whereas a 700 × 350 mm bipolar pad was used for the secondary with an air gap of 200 mm. These pads were used since they were already constructed and available in the laboratory. The full dimensions of the pad and its development are discussed in detail in [29]. The two coils in the bipolar secondary pad were connected to two secondary switching regulators using identical topologies as shown in Fig. 11. The dc outputs of both regulators were connected to an electronic load set to constant voltage mode at 300 V to act as a battery. The tuning capacitors are similar to

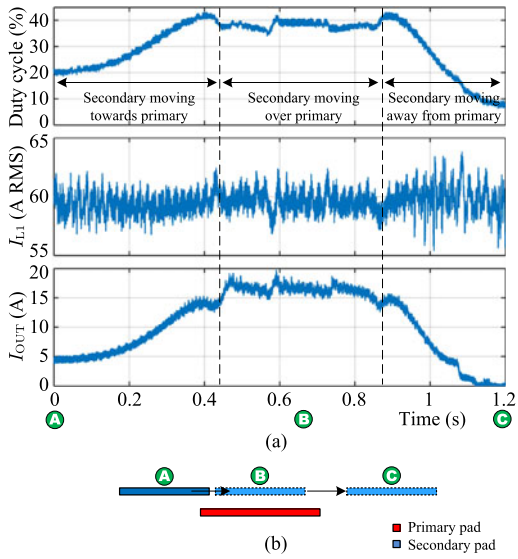

Fig. 16. (a) Oscilloscope traces demonstrating the transient operation of the power supply with a moving secondary pad and (b) position of the moving secondary pad relative to the primary pad at various points in the simulation.

those proposed in Section III-D, however, in order to validate the operation of this power supply under severe mistuning, the value for C_1 is 20% larger than desired so the *LC* tank was tuned to 70 kHz in the worst-case scenario. Despite this, severe mistuning the circuit still operated as expected, however, it lowered the efficiency of the power supply under operation.

Measurements from the experimental system under dynamic operation are shown in Fig. 16(a). Here, key waveforms are shown as the secondary pad moves over the primary pad. To help visualize the position of the secondary pad as it moved over the primary pad, the position of the secondary pad relative to the position of the fixed primary is shown in Fig. 16(b) at the three locations marked A, B, and C on Fig. 16(a). It can be seen that the primary controller regulated the primary current I_{L1} (see Fig. 11) to 60 A rms throughout the experiment. The secondary pad was placed with an initial displacement of 0.66 m away from the center of the primary pad where $I_{OUT} = 5$ A ($P_{OUT} =$ 1.5 kW). The secondary pad was then accelerated along the tracks toward the primary pad. As the secondary pad approached the primary pad, the output current increased to approximately 17 A at which stage the secondary regulator started to regulate

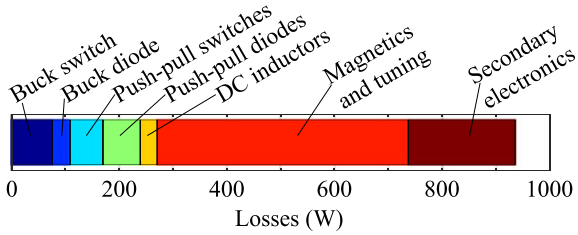

Fig. 17. Distribution of the losses within the system.

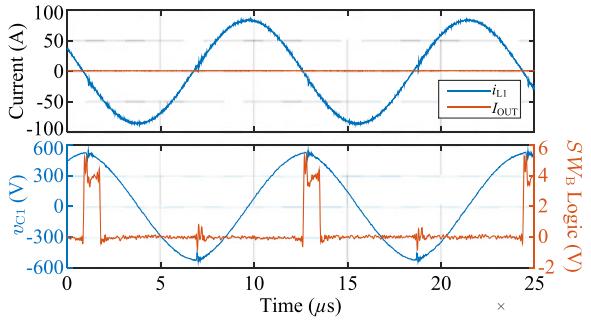

Fig. 18. Oscilloscope waveforms operating at the no load condition.

the output current so that the output power was maintained at 5 kW. Eventually, the secondary pad moved too far away from the primary pad, resulting in the output current dropping to 0 A.

When delivering 5 kW, the system efficiency from the input dc V_{DC} to output dc V_{OUT} ranged from approximately 82.6–84.5% depending on the tuning. When the primary pad was tuned well, a system efficiency of 84.5% was observed. The loss distribution in the system at this operating condition is plotted in Fig. 17 and it can be seen that the losses in the power supply make up approximately 29% of the total losses. For the system to operate well under dynamic conditions, it is necessary to drive the pads at a high current to ensure that the secondary pad continues to receive power even when it is operating when misaligned laterally between two primary pads. Thus, the majority of the magnetic losses occur within the primary pads due to the high currents. In such dynamic applications, there is little time for both the primary and secondary controllers to adjust their currents in order to optimize their efficiency [1] as is possible with stationary systems since the vehicle can spend as little as 36 ms on every pad if it is travelling at 100 km/h. In practice, it would be desirable that the primary set an appropriate current based on the needs of a vehicle from an advanced knowledge from a backbone intelligent highway system. Of the losses within the primary power supply, 28% is within buck converter switch ($\mathrm{SW_B}$) due to its hard switched operation at 85 kHz. Improving this part of the converter is clearly an important consideration in future work.

The efficiency of the system decreased down to 82.6% when it was operated under the mistuned conditions stated in Table I. The mistuned conditions cause the input current into the push–pull converter I_{PP} shown in Fig. 7 to be higher, resulting in more losses within switches, diodes, and the dc inductors of the primary power supply. This result is in line with the simulation results predicted in Fig. 10.

Oscilloscope traces of the system working at the no load condition are shown in Fig. 18. To achieve this no load condition, $\mathrm{SW_{O1}}$ and $\mathrm{SW_{O2}}$ were permanently closed so that I_{OUT} is 0 A. Under these conditions, the system is extremely sensitive to mistuning as shown in Fig. 10 so the duty cycle needed to be low. As shown in the oscilloscope traces, the primary current I_{L1} is regulated to 60 A using a low-duty cycle of 8%.

Overall, the proposed topology has demonstrated the ability to operate under extreme mistuning at the cost of extra losses within the power supply. In this paper, the design of the power supply was deliberately constrained by using a fixed value tuning capacitor and operating at a fixed frequency. The SAE J2954 guidelines [5] allows operation between 81.39 and 90 kHz so this range of frequencies could potentially also be used to reduce the mistuning of the circuit, however, this may introduce additional complexities under dynamic charging conditions that needs further investigation. Furthermore, the tuning of the *LC* tank could potentially be directly adjusted as described in [12] by varying the tuning capacitor C_1 if the circuit is heavily mistuned with a switchable capacitor branch.

VI. Conclusion

In this paper, a system was presented for an inductive power transfer power supply utilizing a buck converter and a fixed frequency unidirectional switch push–pull converter. It required just one extra switch and diode on top of a USPP to implement the extra controllability. With this configuration, it was shown that the circuit was able to offer tolerance to extreme mistuning while maintaining a constant primary current with low distortion. The circuit was able to satisfactorily operate with both inductive and capacitive mistuning. The limitations of the proposed power supply have been explored, and dynamic charging simulations showing the operation of the power supply with a secondary pad moving at 108 km/h was presented. Control schemes to discuss safe start up and shut down have also been discussed together with shut down procedures under fault conditions. Experimental results from a 5-kW dynamic charging prototype have been presented to validate its ability to operate under severe mistuning under dynamic conditions.

References

[1] G. A. Covic and J. T. Boys, "Modern trends in inductive power transfer for transportation applications," *IEEE J. Emerg. Sel. Topics Power Electron.*, vol. 1, no. 1, pp. 28–41, Mar. 2013.

[2] T. Diekhans and R. W. De Doncker, "A dual-side controlled inductive power transfer system optimized for large coupling factor variations and partial load," *IEEE Trans. Power Electron.*, vol. 30, no. 11, pp. 6320–6328, Nov. 2015.

[3] N. Liu and T. G. Habetler, "Design of a universal inductive charger for multiple electric vehicle models," *IEEE Trans. Power Electron.*, vol. 30, no. 11, pp. 6378–6390, Nov. 2015.

[4] H. H. Wu, A. Gilchrist, K. D. Sealy, and D. Bronson, "A high efficiency 5 kW Inductive charger for EVs using dual side control," *IEEE Trans. Ind. Informat.*, vol. 8, no. 3, pp. 585–595, Aug. 2012.

[5] *Wireless Power Transfer for Light-Duty Plug-In/ Electric Vehicles and Alignment Methodology*. SAE TIR J2954_201605, 2016.

[6] L. Chen, G. R. Nagendra, J. T. Boys, and G. A. Covic, "Double-coupled systems for IPT roadway applications," *IEEE J. Emerg. Sel. Topics Power Electron.*, vol. 3, no. 1, pp. 37–49, Mar. 2015.
[7] S. Y. Choi, S. Y. Jeong, B. W. Gu, G. C. Lim, and C. T. Rim, "Ultraslim S-type power supply rails for roadway-powered electric vehicles," *IEEE Trans. Power Electron.*, vol. 30, no. 11, pp. 6456–6468, Nov. 2015.
[8] J. M. Miller *et al.*, "Demonstrating dynamic wireless charging of an electric vehicle: The benefit of electrochemical capacitor smoothing," *IEEE Power Electron. Mag.*, vol. 1, no. 1, pp. 12–24, Mar. 2014.
[9] J. H. Kim *et al.*, "Development of 1-MW inductive power transfer system for a high-speed train," *IEEE Trans. Ind. Electron.*, vol. 62, no. 10, pp. 6242–6250, Oct. 2015.
[10] J. Huh, S. W. Lee, W. Y. Lee, G. H. Cho, and C. T. Rim, "Narrow-width inductive power transfer system for online electrical vehicles," *IEEE Trans. Power Electron.*, vol. 26, no. 12, pp. 3666–3679, Dec. 2011.
[11] V. X. Thai, S. Y. Choi, B. H. Choi, J. H. Kim, and C. T. Rim, "Coreless power supply rails compatible with both stationary and dynamic charging of electric vehicles," in *Proc. 2015 IEEE 2nd Int. Future Energy Electron. Conf.*, Nov. 2015, pp. 1–5.
[12] A. Kamineni, G. A. Covic, and J. T. Boys, "Self-tuning power supply for inductive charging," *IEEE Transactions on Power Electronics*, to be pblished.
[13] H. Hao, G. A. Covic, and J. T. Boys, "An approximate dynamic model of LCL-T-based inductive power transfer power supplies," *IEEE Trans. Power Electron.*, vol. 29, no. 10, pp. 5554–5567, Oct. 2014.
[14] U. K. Madawala, M. Neath, and D. J. Thrimawithana, "A power-frequency controller for bidirectional inductive power transfer systems," *IEEE Trans. Ind. Electron.*, vol. 60, no. 1, pp. 310–317, Jan. 2013.
[15] H. Hao, G. A. Covic, and J. T. Boys, "A parallel topology for inductive power transfer power supplies," *IEEE Trans. Power Electron.*, vol. 29, no. 3, pp. 1140–1151, Mar. 2014.
[16] M. M. Peretz and S. Ben-Yaakov, "Analysis of the current-fed push-pull parallel resonant inverter implemented with unidirectional switches," in *Proc. IEEE 36th Power Electron. Spec. Conf.*, Jun. 2005, pp. 880–884.
[17] A. P. Hu, "Selected resonant converters for IPT power supplies," Ph.D. dissertation, Dept. Elect. Electron. Eng., Univ. Auckland, New Zealand, 2001.
[18] A. W. Green, "Modelling a push-pull parallel resonant convertor using generalised state-space averaging," *Inst. Electr. Eng. Proc. B Elect. Power Appl.*, vol. 140, no. 6, pp. 350–356, Nov. 1993.
[19] C.-S. Wang, G. A. Covic, and O. H. Stielau, "Power transfer capability and bifurcation phenomena of loosely coupled inductive power transfer systems," *IEEE Trans. Ind. Electron.*, vol. 51, no. 1, pp. 148–157, Feb. 2004.
[20] F. Y. Lin, G. A. Covic, and J. T. Boys, "Evaluation of magnetic pad sizes and topologies for electric vehicle charging," *IEEE Trans. Power Electron.*, vol. 30, no. 11, pp. 6391–6407, Nov. 2015.
[21] M. Budhia, J. T. Boys, G. A. Covic, and C. Y. Huang, "Development of a single-sided flux magnetic coupler for electric vehicle IPT charging systems," *IEEE Trans. Ind. Electron.*, vol. 60, no. 1, pp. 318–328, Jan. 2013.
[22] A. Zaheer, H. Hao, G. A. Covic, and D. Kacprzak, "Investigation of multiple decoupled coil primary pad topologies in lumped IPT systems for interoperable electric vehicle charging," *IEEE Trans. Power Electron.*, vol. 30, no. 4, pp. 1937–1955, Apr. 2015.
[23] A. Zaheer, G. A. Covic, and D. Kacprzak, "A bipolar pad in a 10-kHz 300-W distributed IPT system for AGV applications," *IEEE Trans. Ind. Electron.*, vol. 61, no. 7, pp. 3288–3301, Jul. 2014.
[24] J. T. Boys, G. A. Covic, and A. W. Green, "Stability and control of inductively coupled power transfer systems," *Inst Electr. Eng.Proc. — Elect. Power Appl.*, vol. 147, no. 1, pp. 37–43, Jan. 2000.
[25] A. Kamineni, M. J. Neath, A. Zaheer, G. A. Covic, and J. T. Boys, "Interoperable EV detection for dynamic wireless charging with existing hardware and free resonance," *IEEE Transactions on Transportation Electrification*, to be published.
[26] G. R. Nagendra, L. Chen, G. A. Covic, and J. T. Boys, "Detection of EVs on IPT highways," *IEEE J. Emerg. Sel. Topics Power Electron.*, vol. 2, no. 3, pp. 584–597, Sep. 2014.
[27] J. T. Boys, "Vehicle or moving object detection," WO Patent App. PCT/NZ2013/000,202, May 15, 2014.
[28] L. A. Klein, M. K. Mills, and D. R. P. Gibson, *Traffic Detector Handbook*, IIIrd Ed., vol. I., Washington, DC, USA: Federal Highway Administration, U.S. Dept., 2006, Publication Number: FHWA-HRT-06-108.
[29] A. Zaheer, M. J. Neath, H. Z. Beh, and G. A. Covic, "A dynamic EV charging system for slow moving traffic applications," *IEEE Transactions on Transportation Electrification*, to be published.

Abhilash Kamineni (S'10) received the B.E. (Hons.) degree in electrical and electronic engineering from the University of Auckland, Auckland, New Zealand, in 2012, where he is currently working toward the Ph.D. degree in electrical and electronic engineering.

His current research interests include the design and analysis of inductive power transfer systems and developing the power electronic circuits for electric vehicle charging in both stationary and dynamic scenarios.

Michael J. Neath (S'08) received the B.E. (Hons.) and Ph.D. degrees in electrical and electronic engineering from the University of Auckland, Auckland, New Zealand, in 2011 and 2015, respectively.

He is currently a Research Fellow with the University of Auckland. His current research interests include the fields of power electronics, wireless electric vehicle charging, and roadway-powered electric vehicles.

Grant A. Covic (S'88–M'89–SM'04) received the B.E. (Hons.) and Ph.D. degrees in electrical and electronic engineering from the University of Auckland (UoA), Auckland, New Zealand, in 1986 and 1993, respectively.

He was a Full Time Lecturer in 1992, a Senior Lecturer in 2000, an Associate Professor in 2007, and became a Professor in 2013 in the Electrical and Computer Engineering Department, UoA. In 2010, he cofounded (with Prof. J. Boys) a new global start-up company HaloIPT focusing on electric vehicle (EV) wireless charging infrastructure, which was sold in late 2011. He is currently the Head of Inductive Power Research, UoA and coleads the interoperability subteam within the SAE J2954 wireless charging standard for EVs. His research and consulting interests include power electronics, EV battery charging, and highly resonant inductive (contact-less) power transfer (IPT) from which he has published more than 100 refereed papers in international journals and conferences. He holds a number of U.S. patents with many more pending, from which licenses in specialized application areas of IPT have been granted around the world.

He is a fellow of the Institution of Professional Engineers New Zealand, a fellow of the Royal Society of New Zealand, and (together with Prof. Boys) has been received the New Zealand Prime Ministers Science Prize, the KiwiNet Research Commercialisation Award, and the Vice Chancellors Commercialisation Medal for his work in IPT.

John T. Boys received the M.E. degree in power electronics from the University of Auckland, Auckland, New Zealand, in 1965.

After completing the Ph.D. degree in radio science, he was with SPS technologies for five years before returning to academia as a Lecturer with the University of Canterbury. He moved to Auckland in 1977, where he developed his work in power electronics. He is currently a Distinguished Professor Emeritus in the Department of Electrical and Computer Engineering, University of Auckland, and a Cofounder of HaloIPT. He has published more than 100 papers in international journals and is the holder of more than 40 U.S. patents from which licenses in specialized application areas have been granted around the world. His main research interests include power electronics and electromagnetics for inductive power transfer, where he works with Prof. G. A. Covic.

Dr. Boys is a fellow of the Royal Society of New Zealand and a distinguished fellow of the Institution of Professional Engineers New Zealand.